The energy metabolism of *Cupriavidus necator* in different trophic conditions

Michael Jahn[1,2], Nick Crang[1], Arvid H. Gynnå[1], Deria Kabova[4], Stefan Frielingsdorf[4], Oliver Lenz[4], Emmanuelle Charpentier[2,3], Elton P. Hudson[1]

Affiliation

[1]School of Engineering Sciences in Chemistry, Biotechnology and Health, Science for Life Laboratory, KTH – Royal Institute of Technology, Stockholm, Sweden.

[2]Max Planck Unit for the Science of Pathogens, Berlin, Germany

[3]Humboldt-Universität zu Berlin, Institute for Biology – Molecular Microbiology, Philippstr. 13, D-10115 Berlin, Germany

[4]Department of Chemistry, Technical University Berlin, Germany

Corresponding Authors

Michael Jahn, michael.jahn@scilifelab.se

Elton P. Hudson, paul.hudson@scilifelab.se

Keywords

Cupriavidus necator; *Ralstonia eutropha*; energy metabolism, transposon, knockout library, barcoded library, Tn-BarSeq, gene fitness, substrate limitation, chemostat

Highlights

- a barcoded transposon library was used to assess gene fitness for hydrogenase, formate dehydrogenase and ETC complexes
- the utilization of terminal respiratory complexes is substrate specific
- soluble formate dehydrogenase is more important than membrane-bound FDH

- soluble hydrogenase and membrane-bound hydrogenase are equally utilized
- inactivation of hydrogenase and its accessory genes leads to faster growth
- further experiments demonstrate that this is caused by the relief of protein burden

Summary

The 'knallgas' bacterium *Cupriavidus necator* is attracting interest of the biotech industry due to its extremely versatile metabolism. *C. necator* can use hydrogen or formic acid as an energy source, fixes CO_2 *via* the Calvin–Benson–Bassham (CBB) cycle, and grows well on various other organic acids and sugars. Its three partite genome is notable for its size and manifold duplications of key genes (CBB cycle, hydrogenases, nitrate reductases). Comparatively little is known about which of these enzymes and their cofactors are actually utilized for growth on different energy sources.

Here, we investigated the energy metabolism of *C. necator* H16 by growing a barcoded transposon knockout library on various substrates including hydrogen and formic acid. The fitness contribution of each gene was calculated as the degree of enrichment or depletion of its mutants. Clustering of gene fitness revealed several distinct pathways: 1) Some, but not all, Molybdenum Cofactor biosynthesis genes were essential for growth on formate and nitrate respiration. 2) Soluble formate dehydrogenase (FDH) was the dominant means of formate oxidation, not the membrane-bound FDH. 3) For hydrogenases, both soluble and membrane-bound enzymes were beneficial for lithoautotrophic growth. 4) Of the six terminal respiratory complexes in *C. necator* H16, only some are used and utilization depends on the energy source. 5) Deletion of hydrogenase-related genes boosted growth, and we show that the relief from associated protein cost is responsible for this phenomenon.

This study evaluates the contribution of each of *C. necator*'s genes to fitness in industrially relevant growth regimes. Our results illustrate the genomic redundancy of this generalist bacterium, and may inspire future strategies for strain engineering.

Graphical Abstract

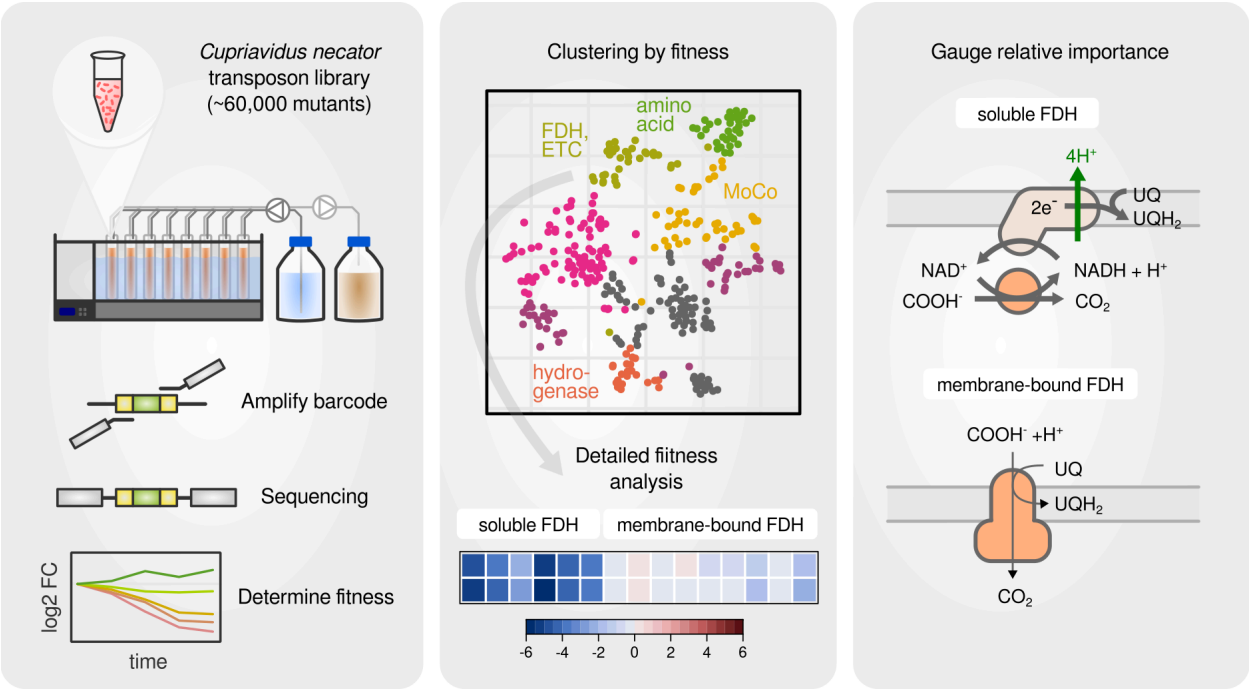

Introduction

The soil bacterium *Cupriavidus necator* (formerly *Ralstonia eutropha*) is a widely recognized model organism for chemolithoautotrophic growth (Bowien & Kusian, 2002, Pohlmann et al., 2006) and for the production of the bioplastic polymer polyhydroxybutyrate (PHB) (Reinecke & Steinbüchel, 2009, Panich et al., 2021). Its large inventory of enzymes enables it to grow on a wide range of heterotrophic substrates as well as on mixtures of molecular oxygen (O_2), molecular hydrogen (H_2), and carbon dioxide (CO_2) (Park et al., 2011). To fuel CO_2 fixation by the Calvin cycle *C. necator* can obtain energy for ATP and reduction equivalents from the oxidation of molecular hydrogen ($H_2 \rightarrow 2e^- + 2H^+$) or formic acid ($HCOOH \rightarrow CO_2 + 2e^- + 2H^+$). Genome redundancy and phylogenetic comparison suggest that the ability for autotrophic growth was recently acquired (Fricke et al., 2009). The large genome (~6,600 genes) is distributed on two chromosomes and one megaplasmid (pHG1) which is significantly smaller than the two chromosomes (Pohlmann et al., 2006). However, pHG1 encodes most of the enzymes associated with lithoautotrophic growth as well as operons that extend metabolic versatility, such as nitrogen fixation and aromatics degradation functions (Schwartz et al., 2003). Both pHG1 and chromosome 2 were likely acquired from other *Burkholderia* species through horizontal gene transfer, while chromosome 1 represents the evolutionarily most ancient DNA molecule (Fricke et al., 2009). In a recent study of the *C. necator* proteome we showed that around 80% of its protein mass is encoded by chromosome 1 irrespective of the growth condition (Jahn et al., 2021). We also showed that conflicts can arise between expression of autotrophic and heterotrophic pathways, leading to suboptimal utilization of resources. One example is the costly expression of Calvin cycle genes during glycolysis which leads to reassimilation of emitted CO_2 (Shimizu et al., 2015, Subagyo et al., 2021), a process that is unlikely to have a biomass yield or growth rate benefit (Jahn et al., 2021). Another example of suboptimality is the redundancy of Calvin cycle enzymes which are encoded by two largely identical *cbb* operons on pHG1 and chromosome 2. Knocking out genes from either copy had no negative effect on autotrophic growth; the second *cbb* copy is therefore completely dispensable (Windhövel & Bowien, 1990, Jahn et al., 2021).

What remains less explored is *C. necator*'s energy metabolism reviewed by Cramm, 2009. In addition to generating ATP through glycolysis (Entner-Doudoroff pathway), the strictly respiratory bacterium is able to oxidize hydrogen *via* two remarkable oxygen-tolerant metalloenzymes, a soluble and a membrane-bound [NiFe]-hydrogenase (SH and MBH, respectively) (Lenz et al., 2018). The maturation of hydrogenases requires dedicated helper

proteins (*hyp* genes) that synthesize and insert the Ni-Fe-$(CN)_2$-CO cofactor into the enzymes (Böck et al., 2006, Bürstel et al., 2012, Schulz et al., 2019). A similar set of enzymes exist for the oxidation of formate, the soluble and membrane-bound formate dehydrogenases (SFDH and MFDH, respectively) (Cramm, 2008). The reaction mechanism of these enzymes is different and they require a Molybdenum cofactor (MoCo) (Maia et al., 2015, Hille et al, 2020).

The soluble (de-)hydrogenases transfer electrons directly to NAD+ generating reducing power in the form of NADH. Membrane-bound (de-)hydrogenases couple the oxidation reaction to the reduction of a universal quinone e^- carrier that is itself used to fuel the electron transport chain and thereby drives proton motive force. The electron transport chain of *C. necator* is highly complex (Cramm, 2008). Whereas *E. coli* has a total of three respiratory complexes, *C. necator* has no fewer than nine (three copies of bo_3 quinol oxidases, two copies of *bd* quinol oxidase, a bc_1 cytochrome reductase, and three different terminal cytochrome oxidases, bb_3, cbb_3, and aa_3) (Cramm, 2008). These complexes are named after the different types of heme cofactors they contain and differ in their biochemical properties such as a) type of the e^- donor and acceptor, b) high or low affinity for the terminal e^- acceptor, and c) the number of protons pumped across the cytoplasmic membrane. Little is known about the usage of these complexes in different trophic modes. In addition to using oxygen as the terminal e^- acceptor, *C. necator* also has the ability to respire nitrate and other nitrogen oxides in anaerobic environments. The genes for the four required enzyme complexes (nitrate, nitrite, nitric oxide, and nitrous oxide reductase) are located on pHG1 and expressed only when oxygen is limiting (Kohlmann et al., 2014).

In this study, we investigated which enzymes of energy metabolism contribute most to cell fitness in different growth regimes including heterotrophic growth, lithoautotrophic growth and formatotrophic growth. We focused on two branches of energy metabolism: enzymes supplying reduced cofactors (NADH, quinol) from substrates, and the electron transport chain that consumes the reduced cofactors to generate ATP. We wondered which of the different FDH and hydrogenase genes/operons are most utilized in *C. necator*. Which of the many accessory genes for FDH/hydrogenase maturation are truly required to make functional enzymes? And what are the fitness costs associated with expression of these pathways? To answer these questions we employed a barcoded transposon library (Wetmore et al., 2015, Price et al., 2018) that was recently used to study the versatile carbon metabolism of *C. necator* (Jahn et al., 2021). The mutant library was created by conjugating *C. necator* H16 with an *E. coli* donor strain, yielding around 60,000 individually barcoded transposon integration mutants (Figure 1 A, Wetmore et al., 2015). The barcodes were mapped to their respective genome integration site

using the TnSeq workflow (Barquist et al., 2016) (Figure 1 A). The enrichment or depletion of individual mutants was then tracked by next generation sequencing of the 20 nt barcode (Figure 1 B). We calculated a gene-wise fitness score from mutant abundances that represents the relative importance of a gene for a particular growth condition. The use of barcodes significantly increases the experimental throughput, allowing us to probe a wide range of genes important for the various energy-generating pathways of *C. necator*.

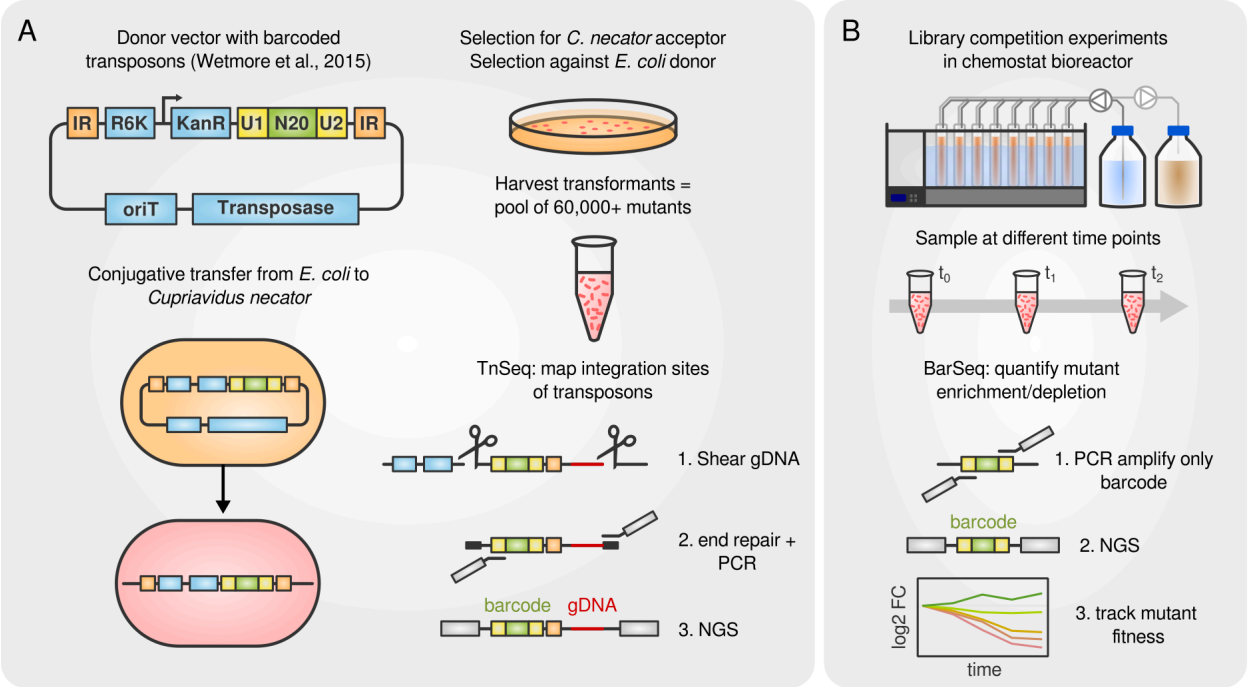

Figure 1: Schematic overview of the creation of the *C. necator* transposon library, and screening workflow. A) *C. necator* H16 was conjugated with an *E. coli* donor strain carrying a transposon integration construct (schematic of vector was adopted from Wetmore et al., 2015). The construct contains inverted repeat (IR) elements that serve as recognition sites for the transposase, an R6K plasmid replication origin, a kanamycin resistance cassette (kanR), two universal priming sites (U1, U2) and the 20 nt random barcode (N20). Transposon integration sites were mapped to barcodes using the TnSeq workflow. Genomic DNA was isolated, shear-fragmented, and end-repaired. Transposon containing fragments were PCR amplified including the barcode and a portion of WT genomic DNA, and then sequenced using NGS. **B)** Library competition experiments were mostly performed in chemostat bioreactors. Samples were taken after a defined number of generations (0, 8, 16), genomic DNA was extracted and barcodes sequenced using NGS. The changes in barcode abundance over time were used to calculate a fitness score for each gene.

Results

Genes involved in energy metabolism dominate fitness screening

We probed the contribution of genes to fitness by growing the transposon mutant library in five different trophic conditions: With fructose, succinate, or formate as carbon and energy source, whereby formate is first oxidized to CO_2 and then fixed *via* the Calvin cycle, furthermore with gas fermentation on CO_2, H_2, and O_2 (lithoautotrophy), and with anoxic growth and nitrate respiration (on fructose). In addition to cultivation with hydrogen (lithoautotrophy), all cultivations were performed with two different feeding regimes, continuous feed (C) and pulsed feed (P), with the intention of promoting either a growth rate or a biomass yield advantage, respectively (Wides & Milo, 2018). We selected all genes with a fitness score $f \leq -2$ or $f \geq 2$ in any condition (354), and clustered genes by similarity (Figure 2 A, Figure S1). The seven emerging clusters were each dominated by genes involved in specific domains: Genes in cluster 1 were almost exclusively related to amino acid biosynthesis and depleted in all growth conditions (Figure 2 B,C). These genes became essential when the mutant library was transitioned from the complete medium of pre-cultures to the minimal medium in bioreactor cultures. Genes in cluster 2 were depleted in formatotrophic growth and strongly enriched for formate dehydrogenases (sorted into 1-carbon metabolism pathways in Figure 2 C) and electron transport complexes. Cluster 3 contained genes related to molybdenum cofactor biogenesis, and mutants were strongly depleted during nitrate respiration. The smallest cluster, number 4, contained almost exclusively genes related to hydrogen metabolism, and its mutants were strongly depleted during lithoautotrophic growth but, surprisingly, enriched in all other conditions. The remaining clusters 5 to 7 were larger, weaker in terms of differential fitness, and more heterogeneous in functional enrichment (Figure 2 C). We therefore focused our analysis on the three energy-related groups formate dehydrogenases, hydrogenases, and the electron transport chain.

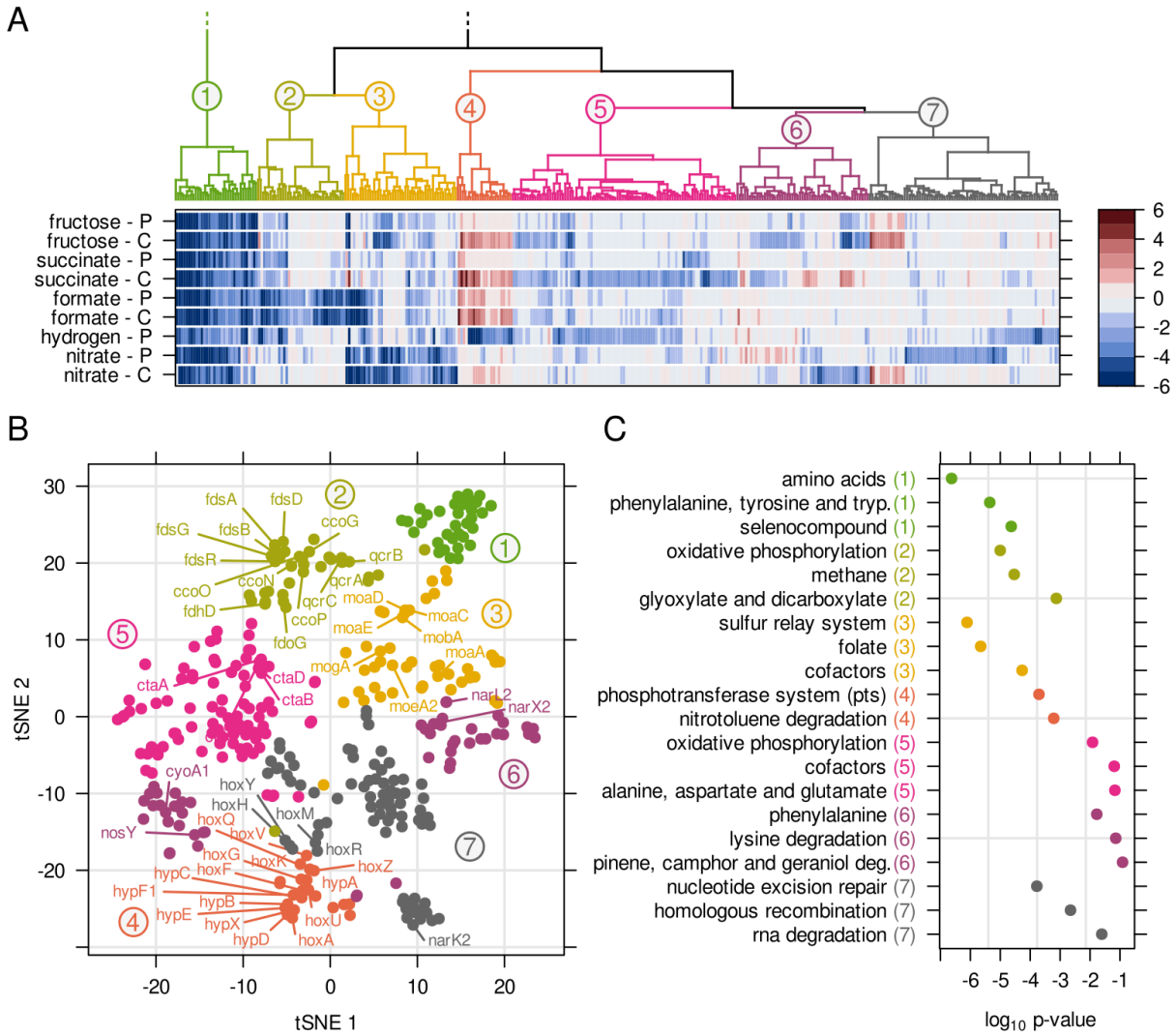

Figure 2: Clustering of genes with significantly changed fitness. A) Fitness scores for 354 genes exceeding a threshold $f \leq -2$ or $f \geq 2$. Genes were clustered based on similarity of fitness scores for the various growth conditions (dendrogram colored by cluster number). An optimal cluster number of 7 was determined using silhouette width, see Figure S1. **B)** t-SNE dimensionality reduction of genes, color coded and labeled by the clusters in A). **C)** Gene enrichment for KEGG pathways. The top three pathways with a p-value lower than 1 were selected. Colors and numbers in brackets indicate the clusters from A).

Fitness related to formate dehydrogenases and their cofactors

The formate dehydrogenases and nitrate reductase of *C. necator* are metalloenzymes that require a molybdenum cofactor (MoCo) which is synthesized using a dedicated pathway (Maia et al., 2015). The basic MoCo molecule is a three-ring aromatic compound, molybdopterin,

which binds a single molybdate anion (MoO_4^{2-}) *via* a dithiolene group (Iobbi-Nivol & Leimkühler, 2013). Four different steps are necessary to synthesize and insert functional MoCo (Iobbi-Nivol & Leimkühler, 2013). In the first step, the molybdopterin backbone is synthesized by cyclization of GTP to cGTP catalyzed by MoaA, conversion to pyranopterin by MoaC, and insertion of two sulfur residues by MoaD and MoaE (Figure 3 A). Only some of these genes are organized in an operon structure on chromosome 1, *moaD*, moa*E* and the MoCo-unrelated fluoride transporter *moaF* (Burgdorf et al., 2001). *MoaA* is located further downstream on chromosome 1 together with *mobA* and *moeA2*. We found that the *moaACDE* genes showed extremely low fitness scores and hence high importance for growth on formate and for nitrate respiration (Figure 3 A). Interestingly, *moaA* (H16_A2581) was only essential for nitrate respiration, but not for formatotrophic growth. A second non-quantified gene copy, *moaA2* (H16_B1466), probably compensates for the *moaA* knockout, suggesting that *moaA* is specific for GTP cyclization during nitrate respiration. The next step in MoCo biosynthesis is the import of the molybdate anion. A dedicated high affinity membrane transport system encoded by *modABC* exists in *C. necator*, but it had no effect on fitness (Figure 3 A). An explanation for this might be the comparatively high concentration of MoO_4^{2-} in the growth medium, permitting transport by other, non-specific transporters (Xia et al., 2018). The molybdate anion is then inserted into molybdopterin through MogA and MoeA (Burgdorf et al., 2001), with MogA increasing the affinity for molybdate at low concentrations without being strictly required (Iobbi-Nivol & Leimkühler, 2013). This was reflected in fitness scores: The *mogA* as well as *moeA1* and *moeA2* knockouts showed somewhat but not dramatically reduced fitness, confirming the non-essentiality of *mogA* and suggesting that *moeA2* can compensate for *moeA1* deletion and *vice versa*. A third *moeA* copy, *moeA3*, showed no change in fitness. Finally, the basic MoCo can be further modified by attaching GTP residues through the action of MobA. The very low fitness score of *mobA* suggests that the GTP modification is strictly essential for FDH and nitrate reductase activity, a feature known from related *E. coli* enzymes of the DMSO reductase family to which *C. necator* S/M-FDH belong (Iobbi-Nivol & Leimkühler, 2013). MobB, whose role in MoCo biosynthesis remains elusive, did not show any fitness effect for its three paralogs *mobB*, *mobB2* and *mobB3*.

The genome of *C. necator* possesses four known operons encoding FDH subunits. The *fdsGBACD* operon encodes the subunits of a soluble, heteromultimeric NAD^+-reducing FDH (Cramm 2008). The *fdsGBA* and *D* mutants showed greatly reduced fitness in formatotrophic growth (Figure 3 B). FdsA, FdsB and FdsG contain iron-sulfur clusters and the molybdenum cofactor, and therefore likely participate in electron transfer. FdsD does not contain any such

cofactor but may assist in maintaining the quaternary structure of the enzyme (Oh & Bowien, 1998, Radon et al., 2020). The role of FdsC remains unclear, but homology analysis suggests it is a sulfur carrier protein that transfers sulfur to MoCo prior to insertion into SFDH (source: https://uniprot.org/unirule/MF_00187). The *fdsC* mutant had moderately reduced fitness, suggesting that it is not strictly essential for growth on formate. However, since the essential subunit *fdsD* is located downstream of *fdsC*, the reduced fitness for *fdsC* may also be caused by a negative effect on *fdsD* expression. Another soluble FDH (*fdwAB*) and two other membrane-bound formate dehydrogenases (MFDH) are annotated but are only poorly functionally characterized. The primary MFDH is encoded by the *fdhABCDE* operon; a secondary three-subunit enzyme is presumably encoded by the *fdoGHI* operon (Cramm 2008). Of these three FDH operons, only the *fdh* operon is located on chromosome 1, while the *fdw* and *fdo* operons are located on chromosome 2, which is thought to have been acquired more recently during evolution (Fricke et al., 2009, Jahn et al., 2021). None of these FDH genes showed a considerable effect on fitness (Figure 3 B), suggesting that the SFDH encoded by the *fds* operon carries by far the main load of formate oxidation.

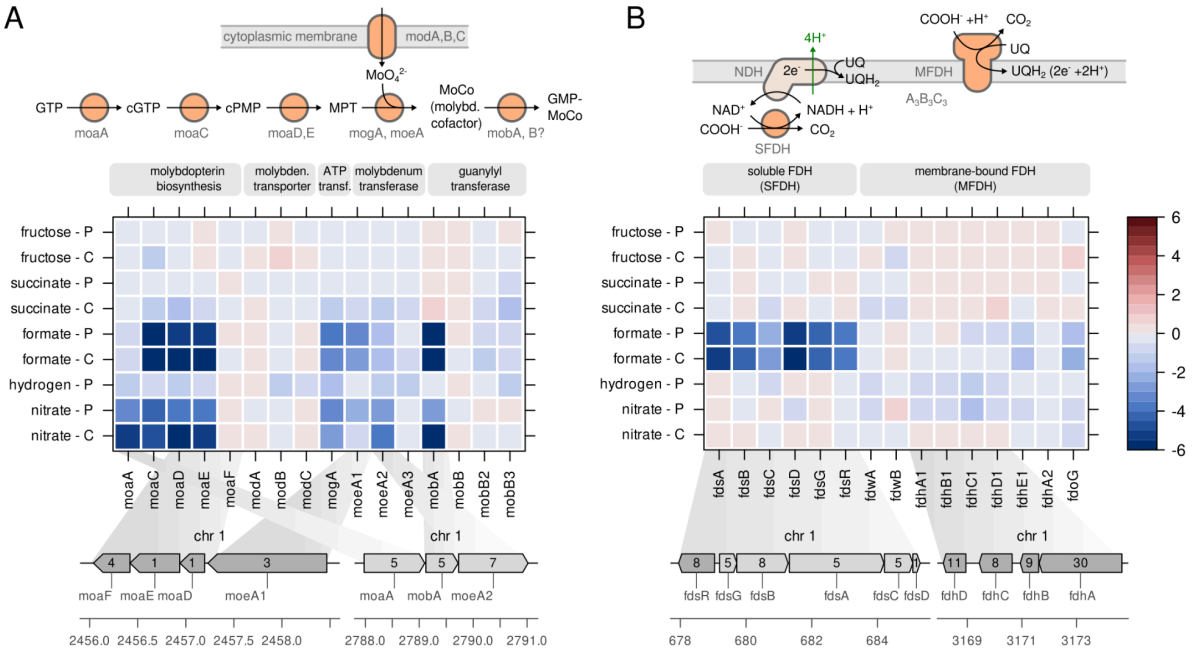

Figure 3: Fitness related to formate dehydrogenases and their cofactors. A) Fitness score for transposon insertion mutants of the molybdenum cofactor (MoCo) biosynthesis pathway. **B)** Fitness score for transposon insertion mutants of various formate dehydrogenase genes. A detailed description can be found in the Results section. The fitness of the *fdoHI* genes was not

quantified. The scale bar indicates the gene fitness score after 8 generations of growth. Inset numbers in genome plots represent the number of transposon mutants per gene. cGTP - cyclic GTP, cPMP - cyclic pyranopterin monophosphate, MPT - molybdopterin, MoCo - molybdopterin cofactor, GMP-MoCo - GMP modified MoCo, SFDH - soluble formate dehydrogenase, MFDH - membrane-bound formate dehydrogenase.

Fitness related to hydrogenases and their cofactors

The *C. necator* hydrogenases are metallo-enzymes that require a nickel-iron-$(CN)_2$-CO cofactor, lending its name to the enzyme class of the [NiFe]-hydrogenases. The metal cofactor is synthesized by a group of accessory Hyp enzymes with genes located on pHG1 (Figure 4 A). The largest operon, *hypA1B1F1C1D1E1X,* is located within an array of hox genes encoding the multi-subunit membrane-bound hydrogenase (MBH, *hoxKGZ*) and regulatory hydrogenase (RH, *hoxABCJ*) (Schwartz et al., 2003). Several partial copies of the *hyp* operon can be found approximately 40 kb downstream in the vicinity of the soluble hydrogenase cluster (*hoxFUYHI*). The function of the *hyp* gene products is well-understood. HypX generates carbon monoxide (CO) from formyl-THF (Schulz et al., 2019), HypEF delivers the cyanide ligands, HypAB delivers the Nickel ion, and HypCD serves as protein scaffold binding the central iron atom that is coordinated by the CN and CO ligands (Bürstel et al., 2012). Fitness data for all *hyp* genes suggest that the primary *hyp* operon is strictly essential for hydrogen assimilation (Figure 4 A), as knockout of these genes led to a dramatic decrease in growth. None of the alternative *hyp* loci were able to rescue primary *hyp[...]1* gene knockout, nor did they have any effect on fitness. However, this result could also be explained by the disruption of *hoxA* transcription, being located directly downstream of *hypX*. Moreover, we observed an unexpected increase in fitness for all *hyp* genes in non-lithoautotrophic conditions. The growth benefit was consistently greater for continuous cultivation (primarily growth rate selective), but still evident in pulsed feed cultivation (primarily yield selective).

The operons encoding the two metabolic hydrogenases, MBH (*hoxKGZ*) and SH (*hoxFUYHI*), are separated by a 75 kb stretch of accessory *hox* and *hyp* genes (Figure 4 B). Inactivation of *hoxKGZ* and *hoxFUYHI* genes led to decreased fitness in lithoautotrophic conditions in all cases, however, fitness was not as strongly decreased as for the *hyp* operon. This indicates that the deficiency in either MBH or SH can be partially compensated for by the activity of the respective other hydrogenase. The genes for a third, non-enzymatic hydrogenase termed the regulatory hydrogenase RH are located between the MBH and SH operons (Figure 4 B, Lenz et al., 2002). The RH (*hoxBC*) is part of a hydrogen-sensing transcriptional regulation system: HoxBC senses the presence of hydrogen and relays this information to the histidine kinase

HoxJ, which phosphorylates HoxA, the master transcriptional regulator. The *C. necator* H16 strain used in this study lost the ability for transcriptional regulation due to a mutation in *hoxJ*, turning *hyp*/*hox* gene expression constantly on (Lenz et al., 2002, Lenz et al., 2018). Accordingly, the function of *hoxB*, *hoxC* and *hoxJ* was dispensable while knockout of *hoxA* led to a dramatic loss of fitness in lithoautotrophic conditions. Fitness of this mutant increased for all other growth conditions similar to *hyp* gene knockout, suggesting that unnecessary hydrogenase expression causes high metabolic cost. The accessory genes *hoxMLOQRTVW* responsible for hydrogenase maturation also showed reduced fitness during autotrophic growth, on a similar scale as that of the main hydrogenase genes.

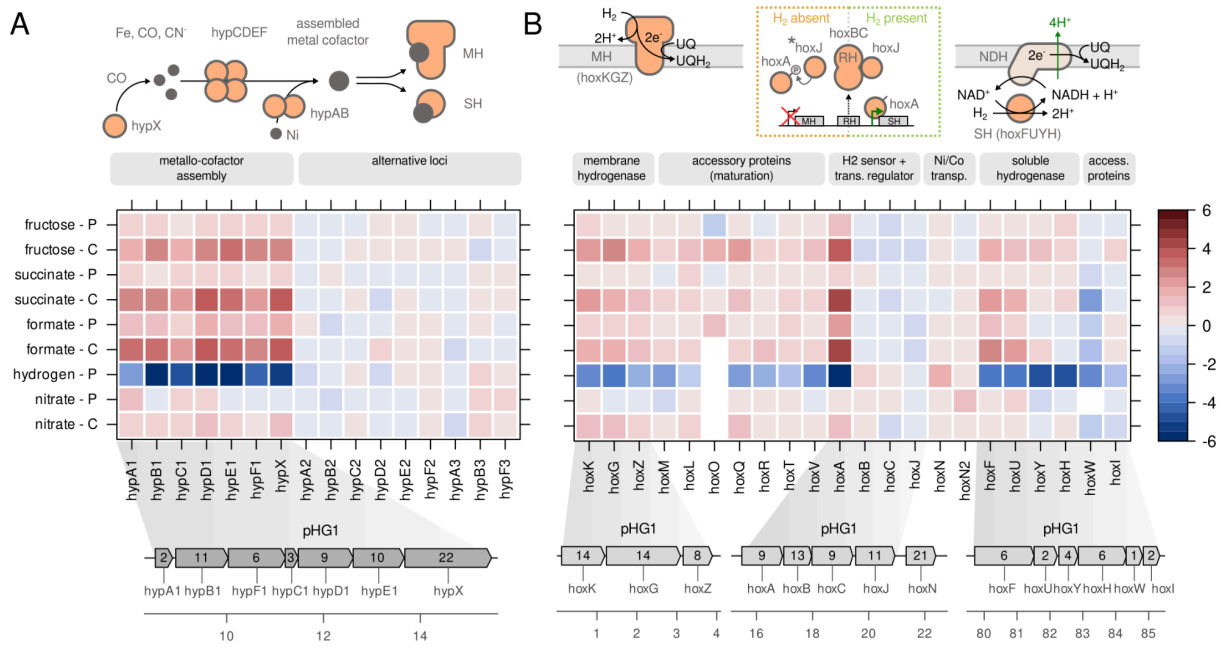

Figure 4: Fitness related to hydrogenases and their cofactors. A) Fitness score for the genes involved in biosynthesis of the Ni-Fe-$(CN)_2$-CO cofactor (*hyp* genes). B) Fitness score for the genes forming membrane-bound hydrogenase (MBH), soluble hydrogenase (SH), regulatory hydrogenase (RH), and accessory genes for maturation of hydrogenases. For details, see the Results section. The scale bar indicates gene fitness scores after 8 generations of growth. Inset numbers in genome plots represent the number of transposon mutants per gene. Asterisk: Note that HoxJ is mutated in the H16 strain and can not regulate HoxA. CO - carbon monoxide, CN^- - cyanide, Ni - nickel, Fe - iron, UQ - ubiquinone, UQH_2 - ubiquinol, NDH - NADH dehydrogenase (complex I).

Fitness related to electron transport chain complexes

C. necator is strictly dependent on respiration in order to generate ATP. Electrons stripped from

a wealth of substrates are either directly transferred (e.g. from MBH, MFDH) to universal electron carriers such as ubiquinone (UQ) or indirectly transferred *via* NADH and the activity of NADH dehydrogenase to UQ. Electrons can then take different paths through the electron transport chain (ETC), generating a proton-motive force across the cytoplasmic membrane that is used to generate ATP through the rotational movement of ATP synthase. Judging by the number of different complexes potentially involved in electron transport, the ETC of *C. necator* is both highly flexible and highly complex (Figure 5). The structural and mechanistic differences of ETC complexes are described in more detail elsewhere (Cramm, 2008, Morris & Schmidt, 2013).

Here we focus on basic functional properties such as electron acceptor affinity and contribution to the proton gradient through proton pumping. The direct route that electrons can take from the e^- donor ubiquinol (UQH_2) to the terminal e^- acceptor oxygen is through the quinol oxidase complexes bo_3 and *bd*. In *C. necator*, the bo_3 complex is encoded by three different *cyoABC* operons and the *bd* complex by two *cydAB* operons (Figure 5). The *bd* family complexes do not pump protons but nevertheless contribute to the membrane potential by consuming two protons through the reduction of O_2 to H_2O at the cytoplasmic side of the membrane (Morris & Schmidt, 2013). Of the bo_3 and *bd* related genes, none showed any significant effect on growth after inactivation. If no duplicate genes compensate for inactivation of the respective targets, it can be assumed that an overwhelming majority of ETC flux takes the alternative route *via* cytochrome reductase (bc_1 complex). *C. necator* has one copy of the bc_1 complex encoded by the *qcrABC* operon and inactivation of any of its genes led to significantly reduced fitness in all conditions except with nitrate as the e^- acceptor (Figure 5). The fitness penalty was highest for formate and lowest for fructose. The bc_1 complex, which is the most abundant ETC complex in *C. necator* (Figure S2), pumps four protons and transfers e^- from UQH_2 to a cytochrome *c* carrier protein.

Cytochrome *c* is then oxidized by one of three complexes, bb_3, aa_3 or cbb_3, all of which transfer the e^- charge to O_2, reducing it to water. Inactivation of the genes encoding the bb_3 complex (*coxMNOPQ*) did not show any effect on fitness. Inactivation of the genes encoding the aa_3 complex (*ctaABCDEG*) on the other hand led to moderately reduced fitness for fructose and succinate, predominantly in pulsed feed conditions. The strongest effect on fitness was observed for genes of the cbb_3 complex (*ccoGNOP*), mainly for growth on formate but not fructose. This suggests that *C. necator* prefers the longer but more energy-efficient route *via* cytochrome reductase and oxidase (4+2 protons pumped per UQH_2), instead of the direct reduction of O_2 through quinol oxidases (2/4 protons pumped per UQH_2). The low O_2 affinity

complex aa_3 was preferred in heterotrophic growth and the high O_2 affinity complex cbb_3 in formatotrophic growth. This result is supported by mass spectrometry data, where the most abundant aa_3 subunit (CtaC) was more abundant in fructose, and the most abundant cbb_3 subunit (CcoO) more abundant in the formate condition (Figure S2).

C. necator also has the ability to respire anoxically using nitrate as the terminal electron acceptor. We probed all four denitrification pathways using our transposon mutant library as described previously (Methods). We verified that the residual oxygen concentration in this setup was minimal (Figure S3) and that the cells were unable to grow anaerobically without nitrate supplementation (Figure S4). Remarkably, nitrate respiration cannot be coupled to formate oxidation (Figure S4B). The *C. necator* genome contains operons for all four steps of denitrification from nitrate (NO_3^-) *via* nitrite (NO_2^-), nitric oxide (NO), nitrous oxide (N_2O) to dinitrogen (N_2), all located on chromosome 2 or pHG1 (Cramm, 2008). Surprisingly, we found no change in fitness for denitrification related genes (Figure S5), whether nitrate was respired or not. The only two exceptions were the regulatory *narX2* and *narL2* mutants, whose fitness was slightly reduced during continuous nitrate respiration. This result is puzzling as it is known that the *nar*, *nir*, *nor* and *nos* operons are strongly upregulated during anaerobic respiration of nitrate, and that the intermediary products of each denitrification step can be detected in *C. necator* (Kohlmann et al., 2014). We assume that gene knockouts were compensated for by other iso-enzymes of the denitrification pathway, thus rescuing the mutants.

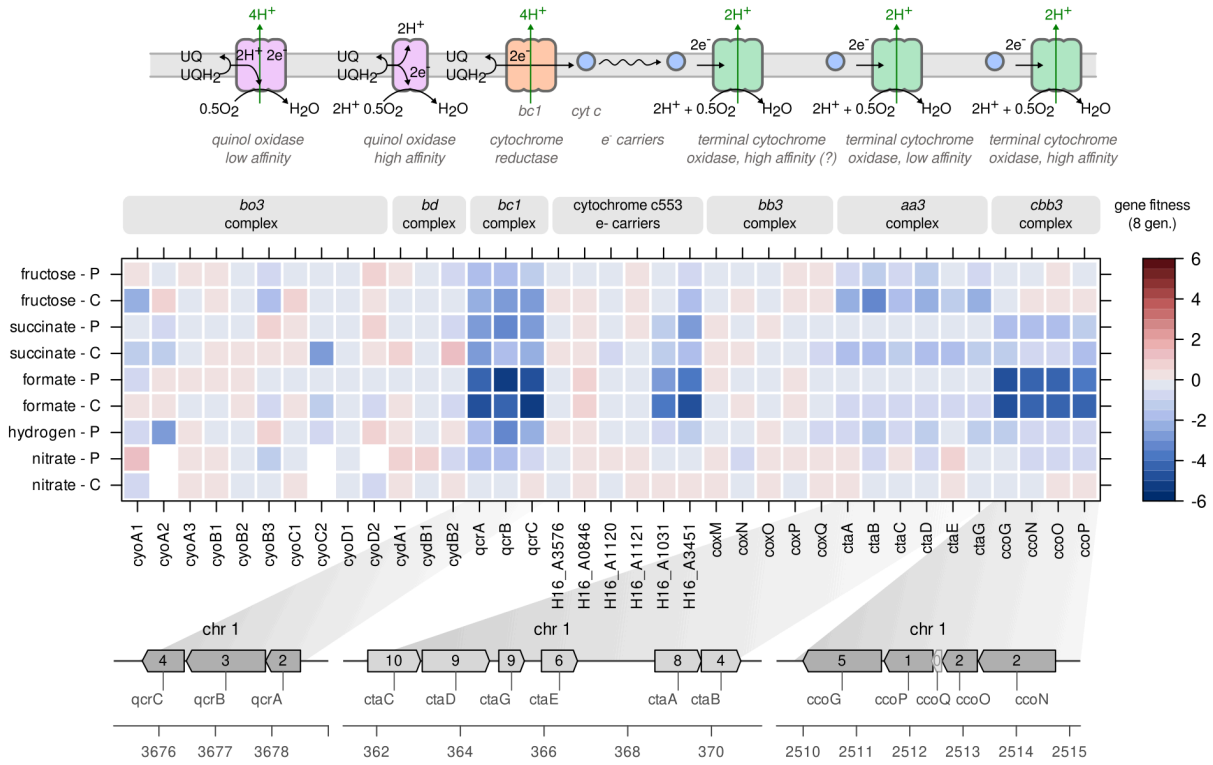

Figure 5: Fitness related to electron transport chain complexes. Fitness score for the genes encoding subunits of different respiratory complexes in the electron transport chain. For details, see the Results section. The scale bar indicates gene fitness scores after 8 generations of growth. Inset numbers in genome plots represent the number of transposon mutants per gene. UQ - ubiquinone, UQH_2 - ubiquinol, e^- - electrons.

Protein cost explains growth advantage of hydrogenase mutants

A surprising result we obtained was the positive fitness score of a range of hydrogenase mutants (Figure 4). We estimated the growth rate advantage of *hox* and *hyp* mutants based on the change of NGS read counts over time (Figure 6 A, Methods). While the absolute increase in growth rate might not be accurate, the differences in growth rate between mutants should be conserved. We found that inactivation of the accessory *hypABCDE* and *hypX* genes as well as inactivation of the master regulator *hoxA* led to an estimated increase in growth rate from 0.1 h^{-1} to 0.12 - 0.14 h^{-1}. Such a pronounced increase in growth rate implies the removal of a considerable burden or cost which is associated with hydrogenase-related genes. We therefore investigated two scenarios, the protein cost hypothesis and the metabolic cost hypothesis, which could explain this observation.

The protein cost hypothesis states that a bacterium is fundamentally limited in its capacity to synthesize proteins (Molenaar 2009, Jahn et al., 2018, Zavrel et al., 2019, Jahn et al., 2021). As a consequence, the utilization of proteins becomes important to optimize growth rate, and every enzyme that is idle constitutes an additional cost. The knockout of an unutilized enzyme leads to a reduction of the protein cost. In order to estimate the *individual* protein cost of hydrogenase related genes, we determined the protein mass fraction for each *hox*/*hyp* enzyme from mass spectrometry data acquired in a previous study (Figure 6 B, Jahn et al., 2021). We then summed up the protein cost for the inactivated gene and all downstream affected genes according to their genomic arrangement and known transcripts, yielding the *total* cost (Figure 6 B, C). For example, inactivation of *hoxK* leads to a low reduction of protein cost because it constitutes only the sum of the protein mass for the lowly expressed *hoxK* to *hoxV* genes. The inactivation of *hoxF* disrupts expression of all SH genes, yielding intermediate reduction of protein cost. Inactivation of *hoxA* on the other hand disrupts the master regulator and silences expression of all *hox* and *hyp* operons, resulting in a strong reduction of protein cost. The *Hyp* gene knockout had the same effect as a *hoxA* knockout, from which we conclude that *hoxA* expression is dependent on the secondary P_{HypA} or P_{HypB} promoters (Lenz et al., 2002). The pattern of total protein cost reduction correlated well with the estimated increase in growth rate (Figure 6 A/B, Figure S6).

To validate the observed fitness advantage, we determined the biomass yield and growth rate of selected in-frame knockout mutants (*hoxG*, *hypB*, *hypX*, *hoxA*, *hoxH*), two mutants for MBH and SH, two for accessory *hyp* genes, and one for the transcriptional regulator HoxA, respectively. The mutants were grown in separate bioreactor batch cultures with fructose as the carbon source, such that hydrogenase expression constitutes a growth burden. Unlike transposon mutatns, these knockouts are not expected to affect expression of downstream genes. We therefore expected the highest increase in biomass yield or growth rate for the *hoxA* mutant, a moderate increase for *hoxH*, and little to no increase for the lowly expressed *hoxG*, *hypB* and *hypX* mutants. The biomass yield was indeed highest for *hoxA*, followed by *hoxH* and hypX, and lower than or equal to WT for *hoxG* and *hypB* (Figure 6 D). The maximum growth rate determined from OD_{720} readings showed an overall similar result (Figure 6 E), with the exception of *hoxA*, for which we expected a higher increase corresponding to the result for biomass yield. However, we noted that the lag phase was shorter for *hoxA*, *hypB* and *hypX* mutants, which could also represent a growth advantage (Figure S7).

Finally, we tested the metabolic cost hypothesis. It proposes that the enzymatic activity of

hydrogenases catalyzes the reverse reaction of H_2 oxidation – the formation of H_2 from protons and an electron donor such as NADH ($2H^+ + 2e^- \rightarrow H_2$). The dissipation of superfluous reducing power in form of NADH is for example known from other microbial phyla such as cyanobacteria, where it is investigated for commercial hydrogen production (Tamagnini et al. 2002, Krishnan et al., 2018). If one of *C. necator*'s hydrogenases generated H_2 while growing heterotrophically, the reaction would drain the NAD(P)H reductant pool and lead to reduced growth. It has been reported that H_2 is being produced when the terminal electron acceptor, oxygen or one of the nitrogen oxides, is limiting (Kuhn et al., 1984). In order to determine if *C. necator* wastes reducing power through the action of hydrogenases, the wild-type H16 strain and a deletion mutant defective in all hydrogenase activity (Δ*hoxG*, Δ*hoxH*, Δ*hoxC* and Δ*hofG*) were cultured in batch with fructose and glycerol to maximize hydrogenase expression (Figure 6 F). No hydrogen evolution was detectable in the absence of strong oxygen limitation. Hydrogen was only detected for the WT strain at the last probed time point (20.5 h) at a concentration of around 1300 ppm (0.13% v/v). Such oxygen-depleted conditions were not present in our bioreactor experiments, ruling out the metabolic cost and strengthening the protein cost hypothesis.

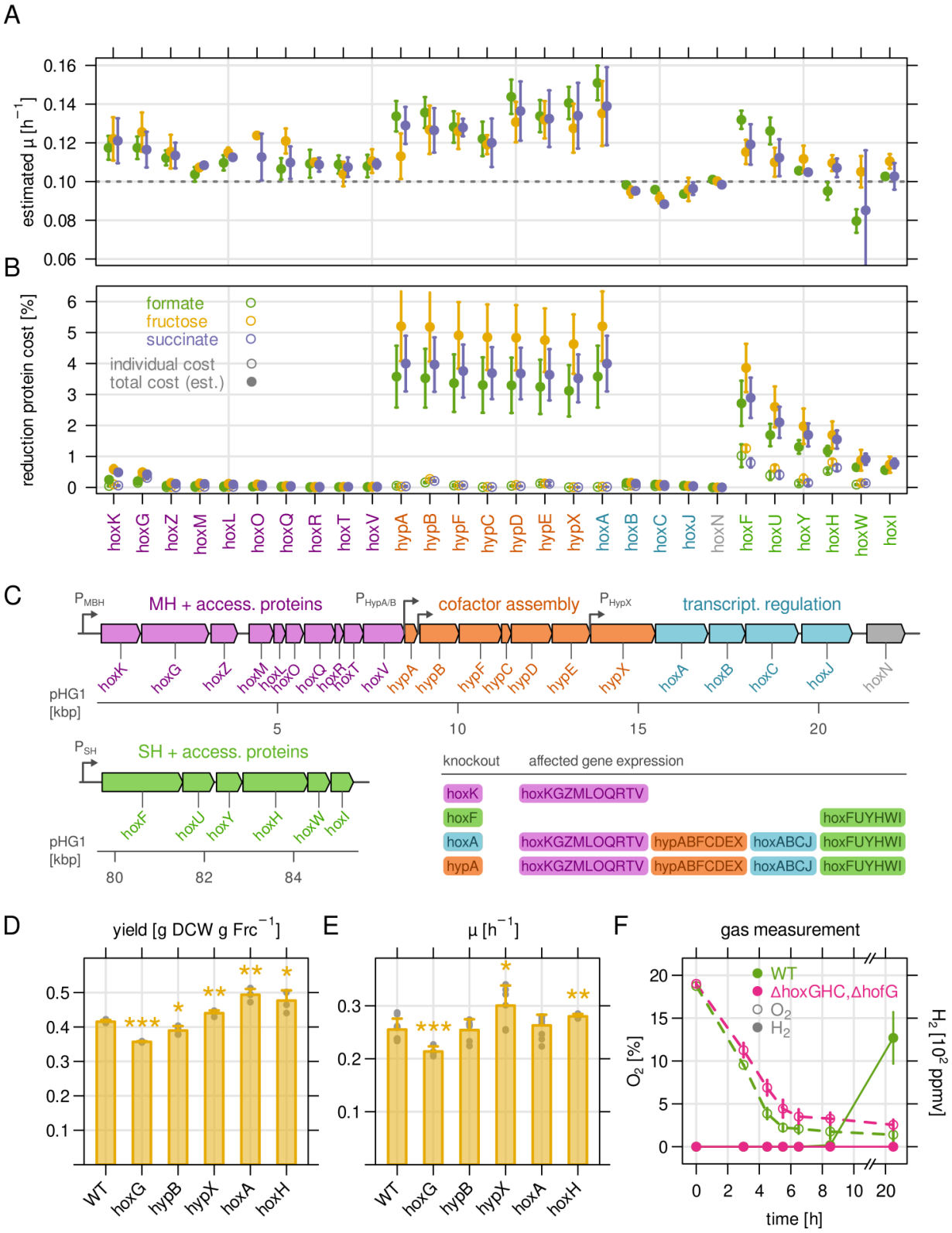
A
estimated μ [h⁻¹]
0.16
0.14
0.12
0.10
0.08
0.06
B
reduction protein cost [%]
formate
fructose
succinate
individual cost
total cost (est.)
hoxK hoxG hoxZ hoxM hoxL hoxO hoxQ hoxR hoxT hoxV hypA hypB hypF hypC hypD hypE hypX hoxA hoxB hoxC hoxJ hoxN hoxF hoxU hoxY hoxH hoxW hoxI
C
P_MBH
MH + access. proteins
P_HypA/B
cofactor assembly
P_HypX
transcript. regulation
pHG1 [kbp]
5
10
15
20
P_SH
SH + access. proteins
80
82
84
knockout
affected gene expression
hoxK hoxKGZMLOQRTV
hoxF hoxFUYHWI
hoxA hoxKGZMLOQRTV hypABFCDEX hoxABCJ hoxFUYHWI
hypA hoxKGZMLOQRTV hypABFCDEX hoxABCJ hoxFUYHWI
D
yield [g DCW g Frc⁻¹]
WT hoxG hypB hypX hoxA hoxH
E
μ [h⁻¹]
F
gas measurement
WT
ΔhoxGHC,ΔhofG
O2
H2
O2 [%]
H2 [10² ppmv]
time [h]

Figure 6: Protein cost explains growth advantage of hydrogenase mutants. **A)** Estimated growth rate μ of hydrogenase-related transposon mutants. The growth rate was calculated from the $\log_2$ fold change in mutant abundance over time compared to the population average. The dashed line marks the nominal growth rate for bioreactor experiments. **B)** Corresponding protein cost for the knockout mutants in A) in percent of the total protein mass. Open symbols, individual cost. Closed symbols, protein cost when disruption of downstream gene expression is taken into account. **C)** Organization of the various hydrogenase-related genes. Membrane-bound hydrogenase MBH (purple), accessory *hyp* genes (orange), and regulatory *hox* genes (blue) are located sequentially on megaplasmid pHG1. Soluble hydrogenase SH is located around 60 kb downstream. Expression of the promoters P_{MBH} and P_{SH} is controlled by the HoxA master regulator. Inset table: Effect on transcription of the selected gene knockouts. It is assumed that knockout of any of the primary *hyp* genes (orange) also disrupts *hoxA* expression. **D)** Biomass yield of selected, in-frame knockout mutants for batch cultures in fructose-supplemented minimal medium. Stars indicate the significance level of a two-sided t-test of each mutant against WT. *, $p \leq 0.05$. **, $p \leq 0.01$. ***, $p \leq 0.001$. **E)** Growth rate directly determined from optical density measurement for the same cultures as in D). **F)** Gas measurements for batch cultures of wild-type *C. necator* H16 (green), and a mutant where all known hydrogenases were knocked out (Δ*hoxG*, Δ*hoxH*, Δ*hoxC* and Δ*hofG*, in red). Open symbols, O_2 measurement. Closed symbols, H_2 measurement. All subfigures: Points and bars represent the mean of at least four biological replicates except F) where three replicates were used. Error bars represent standard deviation.

Discussion

C. necator has attracted interest not only for its ability to produce the storage polymer PHB in high concentrations, but also for its extremely versatile carbon and energy metabolism. Many of the initial groundbreaking studies identifying the key enzymes for its remarkable metabolic capabilities date back to the 1980s and 1990s (Schneider & Schlegel, 1976, Friedrich et al., 1981, Friedebold & Bowien, 1993, Oh & Bowien 1998). Another important milestone was the publication of the full genome sequence (Pohlmann et al., 2006), which made it possible to compile a detailed list of all theoretically present energy acquisition pathways (Cramm, 2008). However, since then most studies on *C. necator* have focused on enhancing PHB production or engineering pathways for biosynthesis of other compounds replacing PHB (Kaddor et al., 2011, Tang et al., 2020, Bommareddy et al., 2020, Janasch et al., 2022). Our study, on the other hand, attempts to build on previous efforts to better understand *C. necator*'s metabolism as a whole.

We have recently studied the carbon metabolism of *C. necator* from the perspective of resource

allocation in different trophic conditions (Jahn et al., 2021). To this end, a barcoded transposon library was created to quantify gene essentiality in the central carbon metabolism, particularly the Calvin cycle which is used for CO_2 fixation. Here, we exploited our knockout library to probe the energy metabolism of *C. necator*. Depletion or enrichment of individual strains thereby revealed the effect of inactivation of a gene on growth rate or biomass yield, which we summarize with the term 'fitness contribution'. Since our data was particularly enriched for specific clusters of genes that affect fitness for formate and hydrogen assimilation as well as the molybdenum cofactor assembly (Figure 2 B), our study focused on these pathways.

The molybdenum cofactor (MoCo) is essential for the function of the two structurally and functionally related enzymes formate dehydrogenase and nitrate reductase (Cramm, 2008). Our results confirmed the essentiality of various enzymes responsible for MoCo biosynthesis. While most enzymes were essential for both formate assimilation and nitrate respiration, *moaA* was only essential for the latter. A second copy, *moaA2*, can probably compensate for this knockout specifically during formatotrophic growth. A set of genes responsible for molybdate anion insertion (*mogA*, *moeA1* and *moeA2*) led to slightly reduced but not completely abolished growth. This confirms that *mogA* is beneficial but not essential (Iobbi-Nivol & Leimkühler, 2013), and that both *moeA* copies are functional and can partially compensate for the knockout of the respective other copy. A third copy, *moeA3*, was hypothesized to play the same role (Cramm, 2008), but our fitness data indicate that this copy is fully dispensable in the conditions tested.

The molybdenum cofactor is an essential component of *C. necator*'s two types of formate dehydrogenases, SFDH and MFDH. The molecular structure and enzymatic mechanism of the main SFDH (*fds* operon) have been studied in great detail (Friedebold et al., 1993, Niks et al., 2016, Hille et al., 2020). Much less is known about the two MFDH enzymes and the second copy of the SFDH, which share only limited similarity on gene level. It is unknown to which extent these formate dehydrogenases are active during formatotrophic growth and whether all or some of them carry metabolic flux. Fitness data from our library experiments clearly suggests that the SFDH of the *fds* operon is the enzyme carrying the main metabolic flux of formate oxidation. All *fds* mutants had strongly reduced fitness while all other FDH mutants did not. In library screenings, we often see a partial decrease in fitness when multiple iso-enzymes with similar activity share the metabolic load (Miao et al., 2023), but the FDH genes did not show such a 'division of labor'. This also means that the overwhelming majority of flux from formate oxidation is channeled towards NADH, and only indirectly towards ubiquinone/ubiquinol in the electron transport chain.

The fitness screening for hydrogenase genes –unlike formate dehydrogenase– suggests that both soluble and membrane-bound hydrogenases are simultaneously utilized for hydrogen oxidation. Mutants for the SH genes *hoxFUYHI* showed moderately reduced fitness scores, similar to the fitness from *hoxKGZ*, while fitness scores for the *hoxA* knockout, which disrupts all *hox* gene expression, were around twice as low. This partial reduction in fitness again suggests that the two iso-enzymes carry roughly equal flux (Miao et al., 2023). The *C. necator* hydrogenases have been of interest for their oxygen tolerance, and have been structurally and functionally well characterized (Saggu et al., 2009, Fritsch et al., 2013). Much less is known about their physiological relevance in different growth conditions. It has been shown that hydrogenase expression is upregulated when the preferred carbon source (e.g. fructose, succinate) is depleted in the culture medium and that expression levels of both hydrogenases are comparable (MBH around 60% of SH, Schwartz et al., 1998, Lenz et al., 2002, Jugder et al., 2015). But the physiological importance in terms of metabolic flux has not yet been quantified. Our results indicate that SH and MBH most likely take a similar share in carrying the metabolic flux from H_2 to reduction equivalents. The SH and MBH enzymes require accessory proteins for biosynthesis of cofactors (*hyp* genes) and maturation (*hoxMLOQRTVW*). Of the three *hyp* operons on pHG1, only the primary *hyp1* operon showed a reduction in fitness. The extremely strong phenotype that was remarkably similar to the *hoxA* mutant suggests however that the KO of these genes disrupts the downstream *hoxA* expression, leading to complete loss of H_2 oxidation capacity. The *hox* maturation genes were all essential for lithoautotrophic growth with the exception of *hoxN/N2*, which encode Nickel transporters (Eitinger & Friedrich, 1991) that are most likely not important when metal concentration in the environment is sufficient.

In formatotrophic or lithoautotrophic lifestyle, redox power generated from formate or H_2 oxidation can take two different routes to fuel the energy requirements of *C. necator*. The NADH from soluble FDH/SH can reduce ubiquinone (UQ) *via* the NADH dehydrogenase (NDH, also known as respiratory complex I). All subunits of NDH are fully essential, as the library contained no transposon mutants of the *nuo* operon encoding them. The second route is the direct transmission of e^- to UQ. The reduced UQH_2 can then be used as a substrate to pump protons by at least three ETC complexes. We found that *C. necator* prefers the route via cytochrome *c* reductase (*qcrABC*), which is 50% more energy efficient in terms of protons pumped (6 vs 2/4), but more complex and therefore likely associated with a higher protein cost. We also found that, of the three annotated terminal cytochrome *c* oxidases, the cbb_3 complex is preferred during formatotrophic growth and the aa_3 complex for growth on fructose. We note that some ETC complexes have different affinity for oxygen, but we only cultivated the library with unlimited O_2

supply (except for nitrate respiration). No complex was clearly essential for growth on hydrogen.

When oxygen is limiting but nitrogen oxides are present, a completely different set of terminal oxidases are used to respire these compounds (Kohlmann et al., 2014) – the dedicated nitrate, nitrite, nitric and nitrous oxide reductase membrane complexes. We grew the transposon library in nitrate respiring conditions and verified that growth without nitrate supplementation did not occur. Yet, we found none of the annotated terminal reductases to be essential. A combination of the following two hypotheses could explain this surprising result: 1) Inactivation of individual denitrification genes can be compensated by one of the many iso-enzymes. For example, a knockout of the primary nitrate reductase (NAR) could be compensated for by the function of either of the two secondary reductases NAP and NAS. In some cases there is no iso-enzyme known, e.g. for nitrite reductase (NIR). 2) Nitrate was present at non-limiting concentration, such that *C. necator* was not dependent on the entire denitrification pathway from nitrate to N_2, making downstream genes non-essential. There were however genes that were conditionally essential for nitrate respiration, the genes for synthesis of the molybdenum cofactor (Figure 2 A). This cofactor is an essential part not only of FDH, but also of all three nitrate reductases (NAR, NAP, NAS), implying that one or more of these enzymes were actively used. We noted that nitrate respiration was impaired when cells were grown on formate instead of fructose (Figure S4). It has previously been reported that *C. necator* cannot respire nitrate when grown lithoautotrophically (Tiemeyer et al., 2007), and this seems to apply to formate as well. Our results did not reveal any hints as to why litho- and formato-autotrophic growth is incompatible with nitrate respiration.

Fitness data for lithoautotrophic growth surprisingly revealed that inactivation of several hydrogenase-related genes boosted growth in heterotrophic conditions. We tested two hypotheses, hydrogenases causing metabolic cost by wasteful conversion of NADH to H_2, or protein cost by production of enzymes (and cofactors). We found that the increase in growth rate was correlated well with the estimated protein mass of hydrogenases and accessory proteins. Moreover, emission of molecular hydrogen that would support the metabolic cost hypothesis was not detected during heterotrophic growth on fructose. The expression of unutilized hydrogenases therefore constitutes a severe growth burden for *C. necator*, at least for strain H16 that was reported to have a defective down-regulation of *hox/hyp* gene expression (Lenz et al., 2002, Lenz et al., 2018). A recent study identified targets for rational engineering of *C. necator* towards faster growth on formate, and reached similar conclusions (Calvey et al., 2023): Of the spontaneous mutations, almost all were deletions of SH, MBH, or the CBB cycle

enzymes whose under-utilization we have described previously (Jahn et al., 2021). The complete removal of the pHG1 megaplasmid encoding all hydrogenases led to one of the biggest improvements in growth rate (Calvey et al., 2023). The increase in maximum growth rate of around 20% for ∆pHG1 corresponds well to the increase of yield or growth rate we observed for selected *hox*/*hyp* mutants, but even more for the growth rate estimated from library experiments (Figure 6). Altogether, our results are in line with the findings from Calvey et al. and mount more evidence for the importance of protein cost in *C. necator*. The tight regulation of hydrogenase expression in strains with functional *hoxJ* signifies the high protein cost associated with litho-autotrophic lifestyle. The detrimental effect of a protein burden on bacterial growth is well-studied in model bacteria (Hui et al., 2015, O'Brien et al., 2016, Mori et al., 2017, Jahn et al., 2018). Microbes nevertheless employ the strategy of keeping enzyme reserves in order to cope with fluctuating environments, changing carbon/energy supply, or stress (Basan et al., 2016, Mori et al., 2017, Jahn et al., 2021). The genome of *C. necator* is well adapted to such a lifestyle, but less suitable for biotechnological application. Our results open up further avenues for the rational engineering of *C. necator*, while other questions, for example the incompatibility of formatotrophy and nitrate respiration, remain open.

Methods

Strains

Cupriavidus necator H16 was obtained from the German Collection of Microorganisms and Cell Cultures, strain number DSM-428. In-frame knockout mutants for *hoxG*, *hypB*, *hypX*, *hoxA* and *hoxH* were obtained from the lab of Oliver Lenz and have been previously described (reference). The negative control strain lacking all four hydrogenases (AH, MBH, RH, SH) was created by serial in-frame deletions of the respective hydrogenase subunit genes. A strain that already carried deletions in the large subunit genes of the MBH, RH, and SH, served as starting point (Schäfer et al., 2013). In this strain, the native AH promoter was already replaced by the MBH promoter. A PCR fragment was amplified with primers 1 and 2 (Table S2), using the megaplasmid pHG1 as a template. The fragment contained the AH large subunit gene *hofG* as well as flanking regions. The fragment was digested with XbaI and subsequently ligated into XbaI-cut pLO1 (Lenz et al., 1994), resulting in the plasmid pGE815. Next, a 1131 bp fragment was removed from the *hofG* gene by restriction using SexAI and subsequent religation, resulting in plasmid pGE816. Double homologous recombination using the suicide vector pGE816

facilitated the incorporation of the *hofG* deletion into the *C. necator* base strain, resulting in a the Δ*hoxG*, Δ*hoxH*, Δ*hoxC*, Δ*hofG* deletion.

Creation of barcoded *C. necator* transposon library

The creation of the barcoded transposon knockout library has been described in detail in Jahn et al., 2021 and Wetmore et al., 2015. Briefly, *C. necator* H16 wild-type was conjugated with an *E. coli* APA766 donor strain containing a barcoded transposon library. The strain is auxotrophic for DAP, the L-Lysin precursor 2,6-diamino-pimelate, to allow for counter selection. Overnight cultures of *E. coli* APA766 and *C. necator* H16 were prepared. The APA766 culture was supplemented with 0.4 mM DAP and 50 µg/mL kanamycin. Fresh cultures were prepared from precultures and then harvested during exponential growth phase by centrifugation for 10 min, 5,000 xg, RT. Supernatant was discarded, cell pellets were resuspended in residual liquid, transferred to 2 mL tubes, washed twice with 2 mL PBS, and finally resuspended in a total amount of 500 µL PBS. Cell suspensions from both strains were combined and plated on 25 cm x 25 cm large trays with LB agar supplemented with 0.4 mM DAP. For conjugation, plates were incubated overnight at 30°C. All cells were then harvested from mating plates by rinsing with PBS and plating on selection plates with LB agar supplemented with 100 µg/mL kanamycin, without DAP. After colonies of sufficient size appeared, transformants were harvested by scraping all cell mass from the plate and collecting the pooled scrapings in 1.5 mL tubes. The mutant library was diluted tenfold and then immediately frozen at -80°C. For competition experiments, a 1 mL 10-fold diluted aliquot (pool of all conjugations, ~1 M CFU) was used to inoculate pre-cultures. The identification of mutant insertion sites ('transposon mapping') is described in detail in Jahn et al., 2021.

Growth medium

Strains were cultivated on complete (LB) medium, or minimal medium depending on experimental setup. Minimal medium was composed of 0.78 g/L NaH_2PO_4, 4.18 g/L $Na_2HPO_4 \times 2H_2O$, 1 g/L NH_4Cl, 0.1 g/L K_2SO_4, 0.1 g/L $MgCl_2 \times 6H_2O$, 1.6 mg/L $FeCl_3 \times 6H_2O$, 0.4 mg/L $CaCl_2$, 0.05 mg/L $CoCl_2 \times 6H_2O$, 1.8 mg/L $Na_2MoO_4 \times 2H_2O$, 0.13 g/L $Ni_2SO_4 \times 6H_2O$, 0.07 mg/L $CuCl_2 \times 2H_2O$. All components were added to autoclaved sodium phosphate buffer from filter-sterilized stock solutions. Standard batch cultures were grown in a volume of 10 to 20 mL medium in 100 mL shake flasks at 30°C and 180 rpm. Precultures of the barcoded *C. necator*

transposon library were supplemented with 200 µg/mL kanamycin and 50 µg/mL gentamicin to suppress growth of untransformed *C. necator* recipient or *E. coli* donor cells.

Pressure bottle cultivation

Pressure bottles were used for batch cultivation in lithoautotrophic or nitrate respiration conditions. For lithoautotrophic growth, precultures of the *C. necator* transposon library were grown overnight in 10 mL LB medium, then transferred to 20 mL of minimal medium containing 2 g/L fructose and 1 g/L NH_4Cl. The precultures were used to inoculate 100 mL Duran Pressure Plus bottles containing 30 mL of minimal medium with 1 g/L ammonium chloride. Samples of the precultures were immediately frozen at -20°C for later use as T0 samples. A GB100 Plus gas mixer (MCQ instruments) paired with a GW-6400-2 anaerobe gas exchange system (GRinstruments) was used to flush and then fill the bottles to a final pressure of 1 bar above standard pressure, with a mixture of 70% H_2, 15% O_2 and 15% CO_2. These culture bottles were shaken at 30°C, 150 rpm. As the cultures approached an OD_{600} of 1.0, they were diluted to OD_{600} of 0.1 and the gas replenished to ensure continuous growth occurred until the end point of 12 or 16 generations of growth were reached. Samples were taken at 4, 8, 12, and 16 generations. For nitrate respiration, the same protocol was used except that the minimal medium was supplemented with 2 g/L fructose, 1 g/L ammonium chloride and 1 g/L $NaNO_3$. Bottles were flushed and then pressurized to 1 bar above standard pressure with 100% N_2.

Bioreactor cultivations

For chemostat experiments, the *C. necator* H16 transposon mutant library was grown as described previously (Jahn et al., 2021). Briefly, an 8-tube MC-1000-OD bioreactor (Photon System Instruments, Drasov, CZ) was customized to perform chemostat cultivation (Jahn et al., 2018, Yao et al., 2020). Bioreactors (65 mL) were filled with minimal medium supplemented with the respective carbon and nitrogen source, and inoculated with an overnight preculture to a target OD_{720nm} of 0.05. Bioreactors were bubbled with air at a rate of 12.5 mL/min and a temperature of 30°C. The OD_{720nm} and OD_{680nm} were measured every 15 min. For chemostat mode, fresh medium was continuously added using Reglo ICC precision peristaltic pumps (Ismatec, GER). For turbidostat mode, the target OD_{720} was set to 0.5 for fructose or 0.2 for formate cultures, and 4 mL medium (6.2% of total volume) was added as soon as the set point was reached. For library competition experiments, 15 mL samples were taken after 0, 8 and 16 generations of growth (population average). Cells were harvested by centrifugation for 10 min at

5,000 xg, 4°C, washed with 1 mL ice-cold PBS, transferred to a 1.5 mL tube, and centrifuged again for 2 min at 8,000 xg, 4°C. The supernatant was discarded and the pellet frozen at -20°C. For batch cultures in the bioreactor, WT or mutant strains were grown using the same setup but with 50 mL volume instead of 65 mL. The entire culture was harvested after the stationary phase was reached to determine the biomass yield.

Biomass yield and growth rate

To determine biomass yield, 50 mL cell suspension was harvested by centrifugation for 10 min, 5,000 xg, 4°C. The pellet was washed twice with 1 mL mqH_2O, transferred to preweighed 1.5 mL tubes and dried for 4 h at 70°C or 55°C overnight. Dried cell mass was measured on a precision scale and yield was calculated according to the equation: yield [gDCW / g substrate] = DCW [mg] / (substrate [g/L] * volume [L] * 1000). Growth rate was calculated by applying a sliding window of 5 hour length to the log OD_{720} over time, and fitting a linear model to each window. The slope of the fitted model was the growth rate for the respective window. From all slopes over time, the maximum was selected as the maximum growth rate.

Hydrogen evolution experiment

Precultures of the H16 wild-type and the hydrogenase negative strain (Δ*hoxG*, Δ*hoxH*, Δ*hoxC*, Δ*hofG*) were grown in FN medium (Lenz et al., 2018) containing 0.4% fructose for 48 h at 37°C and 120 rpm. Main cultures were grown overnight in FGN medium (2 g/L fructose and 2 g/L glycerol) in baffled Erlenmeyer flasks (filled to 20% of the nominal volume) at 30°C and 120 rpm until an optical density at 436 nm (OD_{436}) of approximately 6-8 was reached. The OD_{436} of the culture was adjusted to 6.5 using H16 buffer (C-free minimal medium). The cultures were transferred into 120 mL serum bottles (total bottle volume approx. 147 mL). The bottles were filled with 74 mL of the main culture and thus the gas space was 73 mL and the bottles were subsequently closed airtight with a rubber septum. The bottles were incubated at 30°C and 120 rpm and the gas composition was regularly analyzed by drawing 1 mL of gas from the bottles per measurement using a gas-tight 1-mL Hamilton syringe. The GC measurements followed published protocols (Schäfer et al., 2013).

Gene fitness analysis (BarSeq)

Frozen cell pellets from the pulsed and continuous competition experiments were resuspended in 100 µL of 10 mM Tris and genomic DNA was extracted from 10 µL of the resuspension using

a GeneJet Genomic DNA Purification Kit (ThermoScientific). Amplification of barcodes from genomic DNA was conducted using one of the custom forward indexing primers (BarSeq_F_i7, Table S2) and the reverse phasing primer (BarSeq_R_P2_UMI). For each sample 9 µL of genomic DNA extract (≥10 ng/µL) was combined with 3 µL of a forward indexing primer (100 nM), 3 µL of the reverse phasing primer pool (100 nM) and 15 µL of Q5 Mastermix (New England Biolabs). Cycle conditions were 4 minutes at 98°C followed by 20x (30 seconds at 98°C, 30 seconds at 68°C and 30 seconds at 72°C) with a final extension of 5 minutes at 72°C. Concentration of each sample was quantified using a Qubit dsDNA HS Assay Kit (Invitrogen). Samples were then pooled with 40 ng from up to 36 different samples being combined and run on a 1% agarose gel. Gel extraction was performed on the thick band centered around 200 bp and the concentration of the purified pooled library was quantified again via Qubit assay and diluted to 2 nM. The 2 nM library was then diluted, denatured and sequenced using a NextSeq 500/550 High Output Kit v2.5 (75 Cycles, Illumina) run on an Illumina NextSeq 550 instrument according to the manufacturer's instructions. Library loading concentration was 1.8 pM with a 1% phiX spike. Calculation of gene fitness was performed using the rebar pipeline (https://github.com/m-jahn/rebar, Jahn et al., 2021), which trims and filters reads, extracts barcodes, and summarizes read counts per barcode. Fitness score calculation based on the $\log_2$ fold change of read count per barcode over time was implemented as an R script as part of the pipeline.

Statistical analysis

Bioreactor cultivations, LC-MS/MS measurement for proteomics, and library competition experiments ('BarSeq') were performed with four independent biological replicates. Here, biological replicate means that samples were obtained from independently replicated bottle or bioreactor cultures inoculated with the same preculture. If not otherwise indicated in figure legends, points and error bars represent the mean and standard deviation. No removal of outliers was performed. All analyses of fitness data, cultivations as well as proteomics results are documented in R markdown notebooks available at https://github.com/m-jahn/R-notebook-ralstonia-energy. A significance threshold of $|f| \geq 2$ after at least 8 generations was chosen based on the bulk fitness distribution of mutants. Clustering of genes was performed based on similarity of fitness scores using the R function `hclust()` from package `stats` with method `ward.D2`. Optimal cluster number was determined using silhouette width analysis with the function `silhouette()` from R package `cluster`. T-SNE

dimensionality reduction of genes was performed using R package `tsne`. Gene enrichment for KEGG pathways was performed by using the function `kegga()` from R package `limma`. The R statistical language was used with version 4.3.2.

Data and software availability

Mass spectrometry proteomics data were obtained from the PRIDE repository with the dataset identifier PXD024819. Protein quantification results can be browsed and interactively analyzed using the web application available at https://m-jahn.shinyapps.io/ShinyProt. Sequencing data for BarSeq experiments are available at the European Nucleotide Archive with accession number PRJEB43757. The data for competition experiments performed with the transposon mutant library can be browsed and interactively analyzed using the web application available at https://m-jahn.shinyapps.io/ShinyLib/. All analyses of fitness data, cultivations as well as proteomics results are documented in R notebooks available at https://github.com/m-jahn/R-notebook-ralstonia-energy.

Acknowledgements

We like to thank Ute Hoffmann for support with data submission. This study was financially supported by the Swedish Research Council Vetenskapsrådet (Grant number 2016–06160), the Swedish Research Council Formas (Grant number 2015–939 and 2019–01491), and Novo Nordisk Fonden (Grant number NNF20OC0061469).

References

[1] Barquist L, Mayho M, Cummins C, Cain AK, Boinett CJ, Page AJ, Langridge GC, Quail MA, Keane JA, Parkhill J, The TraDIS toolkit: sequencing and analysis for dense transposon mutant libraries, Bioinformatics, 32, 1109, 2016, doi: 10.1093/BIOINFORMATICS/BTW022, URL /pmc/articles/PMC4896371/pmc/articles/PMC4896371/?report=abstract https://www.ncbi.nlm.nih.gov/pmc/articles/PMC4896371/.

[2] Basan M, Hui S, Okano H, Zhang Z, Shen Y, Williamson JR, Hwa T, Overflow metabolism in Escherichia coli results from efficient proteome allocation, Nature, 528, 99–104, 2015, doi:10.1038/nature15765.

[3] Bommareddy RR, Wang Y, Pearcy N, Hayes M, Lester E, Minton NP, Conradie AV, A Sustainable Chemicals Manufacturing Paradigm Using CO2 and Renewable H2, iScience, 23, 2020, doi:10.1016/J.ISCI.2020.101218, URL https://pubmed.ncbi.nlm.nih.gov/32559729/.

[4] Bowien B, Kusian B, Genetics and control of CO2 assimilation in the chemoautotroph Ralstonia eutropha, 2002, doi:10.1007/s00203-002-0441-3, URL https://link.springer.com/article/10.1007/s00203-002-0441-3.

[5] Burgdorf T, Bömmer D, Bowien B, Involvement of an Unusual mol Operon in Molybdopterin Cofactor Biosynthesis in Ralstonia eutropha, 2001, URL www.caister.com/bacteria-plant.

[6] Böck A, King PW, Blokesch M, Posewitz MC, Maturation of Hydrogenases, Advances in Microbial Physiology, 51, 1–225, 2006, doi:10.1016/S0065-2911(06)51001-X.

[7] Bürstel I, Sieberts E, Winter G, Hummels P, Zebgers I, Friedrich B, Lenz O, A Universal Scaffold for Synthesis of the Fe(CN)2(CO) Moiety of [NiFe] Hydrogenase, Journal of Biological Chemistry, 287, 38845–38853, 2012, doi: 10.1074/JBC.M112.376947.

[8] Calvey CH, i Nogué VS, White AM, Kneucker CM, Woodworth SP, Alt HM, Eckert CA, Johnson CW, Improving growth of Cupriavidus necator H16 on formate using adaptive laboratory evolution-informed engineering, Metabolic engineering, 75, 78–90, 2023, doi:10.1016/J.YMBEN.2022.10.016, URL https://pubmed.ncbi.nlm.nih.gov/36368470/.

[9] Cramm R, Genomic view of energy metabolism in Ralstonia eutropha H16, Journal of Molecular Microbiology and Biotechnology, 16, 38–52, 2008, doi: 10.1159/000142893.

[10] Eitinger T, Friedrich B, Cloning, Nucleotide Sequence, and Heterologous Expression of a High-affinity Nickel Transport Gene from Alcaligenes eutrophus", Journal of Biological Chemistry, 266, 3222–3227, 1991, doi:10.1016/S0021-9258(18)49977-2.

[11] Fricke WF, Kusian B, Bowien B, The Genome Organization of Ralstonia eutropha Strain H16 and Related Species of the Burkholderiaceae, J Mol Microbiol Biotechnol, 16, 124–135, 2009, doi:10.1159/000142899.

[12] Friedebold J, Bowien B, Physiological and Biochemical Characterization of the Soluble Formate Dehydrogenase, a Molybdoenzyme from Alcaligenes eutrophus, 1993, URL https://journals.asm.org/journal/jb.

[13] Friedrich B, Hogrefe C, Schlegel HG, Naturally occurring genetic transfer of hydrogen-oxidizing ability between strains of Alcaligenes eutrophus., Journal of Bacteriology, 147, 198–205, 1981, URL https://jb.asm.org/content/147/1/198.

[14] Fritsch J, Lenz O, Friedrich B, Structure, function and biosynthesis of O2-tolerant hydrogenases, Nature Reviews Microbiology 2013 11:2, 11, 106–114, 2013, doi:10.1038/nrmicro2940, URL https://www.nature.com/articles/nrmicro2940.

[15] Hille R, Young T, Niks D, Hakopian S, Tam TK, Yu X, Mulchandani A, Blaha GM, Structure: Function studies of the cytosolic, Mo-and NAD+ dependent formate dehydrogenase from Cupriavidus necator, 2020, doi: 10.3390/INORGANICS8070041.

[16] Hui S, Silverman JM, Chen SS, Erickson DW, Basan M, Wang J, Hwa T, Williamson JR, Quantitative proteomic analysis reveals a simple strategy of global resource allocation in bacteria, Molecular Systems Biology, 11, 784, 2015, doi:10.15252/msb.20145697.

[17] Iobbi-Nivol C, Leimkühler S, Molybdenum enzymes, their maturation and molybdenum cofactor biosynthesis in Escherichia coli, Biochimica et biophysica acta, 1827, 1086–1101, 2013, doi:10.1016/J.BBABIO.2012.11.007,
URL https://pubmed.ncbi.nlm.nih.gov/23201473/.

[18] Jahn M, Crang N, Janasch M, Hober A, Forsström B, Kimler K, Mattausch A, Chen Q, Asplund-Samuelsson J, Hudson EP, Protein allocation and utilization in the versatile chemolithoautotroph Cupriavidus necator, eLife, 10, 2021, doi:10.7554/ELIFE.69019, URL https://elifesciences.org/articles/69019.

[19] Jahn M, Vialas V, Karlsen J, Maddalo G, Edfors F, Forsström B, Uhlén M, Käll L, Hudson EP, Growth of Cyanobacteria Is Constrained by the Abundance of Light and Carbon Assimilation Proteins, Cell Reports, 25, 478–486.e8, 2018, doi:10.1016/j.celrep.2018.09.040,
URL https://linkinghub.elsevier.com/retrieve/pii/S2211124718314852.

[20] Janasch M, Crang N, Asplund-Samuelsson J, Sporre E, Bruch M, Gynnå A, Jahn M, Hudson EP, Thermodynamic limitations of PHB production from formate and fructose in Cupriavidus necator, Metabolic Engineering, 73, 256–269, 2022, doi:10.1016/J.YMBEN.2022.08.005.

[21] Jugder BE, Chen Z, Ping DTT, Lebhar H, Welch J, Marquis CP, An analysis of the changes in soluble hydrogenase and global gene expression in Cupriavidus necator (Ralstonia eutropha) H16 grown in heterotrophic diauxic batch culture, Microbial Cell Factories, 14, 1–11, 2015, doi:10.1186/s12934-015-0226-4.

[22] Kaddor C, Steinbüchel A, Effects of homologous phosphoenolpyruvate-carbohydrate phosphotransferase system proteins on carbohydrate uptake and poly(3-Hydroxybutyrate) accumulation in Ralstonia eutropha H16, Applied and Environmental Microbiology, 77, 3582–3590, 2011, doi: 10.1128/AEM.00218-11.

[23] Kohlmann Y, Pohlmann A, Schwartz E, Zühlke D, Otto A, Albrecht D, Grimmler C, Ehrenreich A, Voigt B, Becher D, Hecker M, Friedrich B, Cramm R, Coping with Anoxia: A Comprehensive Proteomic and Transcriptomic Survey of Denitrification, Journal of Proteome Research, 13, 4325–4338, 2014, doi:10.1021/pr500491r, URL https://pubs.acs.org/doi/10.1021/pr500491r.

[24] Krishnan A, Qian X, Ananyev G, Lun DS, Dismukes GC, Rewiring of cyanobacterial metabolism for hydrogen production: Synthetic biology approaches and challenges, Advances in Experimental Medicine and Biology, 1080, 171–213, 2018, doi:10.1007/978-981-13-0854-3-8/FIGURES/10,
URL https://link.springer.com/chapter/10.1007/978-981-13-0854-3-8.

[25] Kuhn M, Steinbüchel A, Schlegel HG, Hydrogen Evolution by Strictly Aerobic Hydrogen Bacteria Under Anaerobic Conditions, Journal of Bacteriology, 159, 633–639, 1984, doi:doi.org/10.1128/jb.159.2.633-639.1984, URL https://journals.asm.org/journal/jb.

[26] Lenz O, Bernhard M, Buhrke T, Schwartz E, Friedrich BR, The Hydrogen-Sensing Apparatus in Ralstonia eutropha, Journal of Molecular Microbiology and Biotechnology, 4, 255–262, 2002, URL https://pubmed.ncbi.nlm.nih.gov/11931556/.

[27] Lenz O, Lauterbach L, Frielingsdorf S, O2-tolerant [NiFe]-hydrogenases of Ralstonia eutropha H16: Physiology, molecular biology, purification, and biochemical analysis, Methods in Enzymology, 613, 117–151, 2018, doi:10.1016/BS.MIE.2018.10.008, URL https://pubmed.ncbi.nlm.nih.gov/30509463/.

[28] Maia LB, Moura JJ, Moura I, Molybdenum and tungsten-dependent formate dehydrogenases, Journal of Biological Inorganic Chemistry, 20, 287–309, 2015, doi:10.1007/S00775-014-1218-2/FIGURES/9,
URL https://link.springer.com/article/10.1007/s00775-014-1218-2.

[29] Miao R, Jahn M, Shabestary K, Peltier G, Hudson EP, CRISPR interference screens reveal growth–robustness tradeoffs in Synechocystis sp. PCC 6803 across growth conditions, The Plant Cell, 35, 3937–3956, 2023, doi:10.1093/PLCELL/KOAD208, URL https://dx.doi.org/10.1093/plcell/koad208.

[30] Molenaar D, Berlo RV, Ridder DD, Teusink B, Shifts in growth strategies reflect tradeoffs in cellular economics, Molecular Systems Biology, 5, 1–10, 2009, doi:10.1038/msb.2009.82, URL http://dx.doi.org/10.1038/msb.2009.82.

[31] Mori M, Schink S, Erickson DW, Gerland U, Hwa T, Quantifying the benefit of a proteome reserve in fluctuating environments, Nature Communications, 8, 1–8, 2017, doi:10.1038/s41467-017-01242-8.

[32] Morris RL, Schmidt TM, Shallow breathing: Bacterial life at low O 2, Nature Reviews Microbiology, 11, 205–212, 2013, doi:10.1038/nrmicro2970, URL https://www.ncbi.nlm.nih.gov/pmc/articles/PMC3969821/.

[33] Niks D, Duvvuru J, Escalona M, Hille R, Spectroscopic and Kinetic Properties of the Molybdenum-containing, NAD+-dependent Formate Dehydrogenase from Ralstonia eutropha, The Journal of biological chemistry, 291, 1162–1174, 2016, doi:10.1074/JBC.M115.688457, URL https://pubmed.ncbi.nlm.nih.gov/26553877/.

[34] Oh JI, Bowien B, Structural analysis of the fds operon encoding the NAD+ linked formate dehydrogenase of Ralstonia eutropha, The Journal of biological chemistry, 273, 26349–26360, 1998, doi:10.1074/JBC.273.41.26349, URL https://pubmed.ncbi.nlm.nih.gov/9756865/.

[35] O'Brien EJ, Utrilla J, Palsson BO, Quantification and Classification of E. coli Proteome Utilization and Unused Protein Costs across Environments, PLoS Computational Biology, 12, 1–22, 2016, doi:10.1371/journal.pcbi.1004998.

[36] Panich J, Fong B, Singer SW, Metabolic Engineering of Cupriavidus necator H16 for Sustainable Biofuels from CO2, 2021, doi: 10.1016/j.tibtech.2021.01.001.

[37] Park J, Kim T, Lee S, Genome-scale reconstruction and in silico analysis of the Ralstonia eutropha H16 for polyhydroxyalkanoate synthesis, lithoautotrophic growth, and 2-methyl citric acid production, BMC Systems Biology, 5, 101, 2011, doi:10.1186/1752-0509-5-101, URL http://www.biomedcentral.com/1752-0509/5/101.

[38] Pohlmann A, Fricke WF, Reinecke F, Kusian B, Liesegang H, Cramm R, Eitinger T, Ewering C, Pötter M, Schwartz E, Strittmatter A, Voß I, Gottschalk G, Steinbüchel A, Friedrich B, Bowien B, Genome sequence of the bioplastic-producing "Knallgas" bacterium Ralstonia eutropha H16, Nature Biotechnology, 24, 1257–1262, 2006, doi:10.1038/nbt1244.

[39] Price MN, Wetmore KM, Waters RJ, Callaghan M, Ray J, Liu H, Kuehl JV, Melnyk RA, Lamson JS, Suh Y, Carlson HK, Esquivel Z, Sadeeshkumar H, Chakraborty R, Zane GM, Rubin BE, Wall JD, Visel A, Bristow J, Blow MJ, Arkin AP, Deutschbauer AM, Mutant phenotypes for thousands of bacterial genes of unknown function, Nature, 557, 503–509, 2018, doi:10.1038/s41586-018-0124-0,
URL http://www.nature.com/articles/s41586-018-0124-0.

[40] Radon C, Mittelstädt G, Duffus BR, Bürger J, Hartmann T, Mielke T, Teutloff C, Leimkühler S, Wendler P, Cryo-EM structures reveal intricate Fe-S cluster arrangement and charging in Rhodobacter capsulatus formate dehydrogenase, Nature Communications 2020 11:1, 11,

1–9, 2020, doi:10.1038/s41467-020-15614-0,
URL https://www.nature.com/articles/s41467-020-15614-0.

[41] Reinecke F, Steinbüchel A, Ralstonia eutropha Strain H16 as Model Organism for PHA Metabolism and for Biotechnological Production of Technically Interesting Biopolymers, Microbial Physiology, 16, 91–108, 2009, doi:10.1159/000142897, URL https://www.karger.com/Article/FullText/142897

[42] Saggu M, Zebger I, Ludwig M, Lenz O, Friedrich B, Hildebrandt P, Lendzian F, Spectroscopic Insights into the Oxygen-tolerant Membrane-associated [NiFe] Hydrogenase of Ralstonia eutropha H16, The Journal of Biological Chemistry, 284, 16264, 2009, doi: 10.1074/JBC.M805690200, URL https://www.ncbi.nlm.nih.gov/pmc/articles/PMC2713555/.

[43] Schneider K, Schlegel HG, Purification and properties of soluble hydrogenase from Alcaligenes eutrophus H 16, Biochimica et biophysica acta, 452, 66–80, 1976, doi:10.1016/0005-2744(76)90058-9, URL https://pubmed.ncbi.nlm.nih.gov/186126/.

[44] Schulz AC, Frielingsdorf S, Pommerening P, Lauterbach L, Bistoni G, Neese F, Oestreich M, Lenz O, Formyltetrahydrofolate Decarbonylase Synthesizes the Active Site CO Ligand of O2-Tolerant [NiFe] Hydrogenase, Journal of the American Chemical Society, 142, 1457–1464, 2019, doi:10.1021/JACS.9B11506,
URL https://pubs.acs.org/doi/full/10.1021/jacs.9b11506.

[45] Schwartz E, Gerischer U, Friedrich B, Transcriptional regulation of Alcaligenes eutrophus Hydrogenase genes, Journal of Bacteriology, 180, 3197–3204, 1998, doi: 10.1128/JB.180.12.3197-3204.1998/ASSET/40D9FB9F-4D4A-4E3D-B338-23BE83BDD6BC/ASSETS/GRAPHIC/JB1280065006.JPEG,
URL https://journals.asm.org/doi/10.1128/jb.180.12.3197-3204.1998.

[46] Schwartz E, Henne A, Cramm R, Eitinger T, Friedrich B, Gottschalk G, Complete nucleotide sequence of pHG1: A Ralstonia eutropha H16 megaplasmid encoding key enzymes of H2-based lithoautotrophy and anaerobiosis, Journal of Molecular Biology, 332, 369–383, 2003, doi:10.1016/S0022-2836(03)00894-5.

[47] Schäfer C, Friedrich B, Lenza O, Novel, oxygen-insensitive group 5 [NiFe]-hydrogenase in Ralstonia eutropha, Applied and Environmental Microbiology, 79, 5137–5145, 2013, doi:10.1128/AEM.01576-13.

[48] Shimizu R, Dempo Y, Nakayama Y, Nakamura S, Bamba T, Fukusaki E, Fukui T, New Insight into the Role of the Calvin Cycle: Reutilization of CO2 Emitted through Sugar Degradation, Scientific Reports, 5, 11617, 2015, doi:10.1038/srep11617, URL http://www.nature.com/articles/srep11617.

[49] Subagyo DCH, Shimizu R, Orita I, Fukui T, Isopropanol production with reutilization of glucose-derived CO2 by engineered Ralstonia eutropha, Journal of Bioscience and Bioengineering, 132, 479–486, 2021, doi: 10.1016/J.JBIOSC.2021.08.004.

[50] Tamagnini P, Axelsson R, Lindberg P, Oxelfelt F, Wünschiers R, Lindblad P, Hydrogenases and Hydrogen Metabolism of Cyanobacteria, Microbiology and Molecular Biology Reviews : MMBR, 66, 1, 2002, doi:10.1128/MMBR.66.1.1-20.2002, URL https://www.ncbi.nlm.nih.gov/pmc/articles/PMC120778/.

[51] Tang R, Weng C, Peng X, Han Y, Metabolic engineering of Cupriavidus necator H16 for improved chemoautotrophic growth and PHB production under oxygen-limiting conditions, Metabolic Engineering, 61, 11–23, 2020, doi: 10.1016/j.ymben.2020.04.009.

[52] Tiemeyer A, Link H, Weuster-Botz D, Kinetic studies on autohydrogenotrophic growth of Ralstonia eutropha with nitrate as terminal electron acceptor, Applied Microbiology and Biotechnology, 76, 75–81, 2007, doi:10.1007/s00253-007-0983-z, URL https://link.springer.com/article/10.1007/s00253-007-0983-z.

[53] Wetmore KM, Price MN, Waters RJ, Lamson JS, He J, Hoover CA, Blow MJ, Bristow J, Butland G, Arkin AP, Deutschbauer A, Rapid Quantification of Mutant Fitness in Diverse Bacteria by Sequencing Randomly Barcoded Transposons, mBio, 6, 1–15, 2015, doi:10.1128/mBio.00306-15, URL https://mbio.asm.org/content/6/3/e00306-15.

[54] Wides A, Milo R, Understanding the Dynamics and Optimizing the Performance of Chemostat Selection Experiments, arXiv. 2018, doi: https://doi.org/10.48550/arXiv.1806.00272.

[55] Windhövel U, Bowien B, On the operon structure of the cfx gene clusters in Alcaligenes eutrophus, Archives of microbiology, 154, 85–91, 1990, doi:10.1007/BF00249183, URL https://pubmed.ncbi.nlm.nih.gov/2168696/.

[56] Xia Z, Lei L, Zhang HY, Wei HL, Characterization of the ModABC molybdate transport system of pseudomonas putida in nicotine degradation, Frontiers in Microbiology, 9, 2018, doi: 10.3389/FMICB.2018.03030/FULL, URL https://www.ncbi.nlm.nih.gov/pmc/articles/PMC6295455/.

[57] Yao L, Shabestary K, Björk S, Asplund-Samuelsson J, Joensson H, Jahn M, Hudson E, Pooled CRISPRi screening of the cyanobacterium Synechocystis sp PCC 6803 for enhanced industrial phenotypes, Nature Communications, 11, 1–13, 2020, doi:10.1101/823534, URL https://www.nature.com/articles/s41467-020-15491-7.

[58] Zavřel T, Faizi M, Loureiro C, Poschmann G, Stühler K, Sinetova M, Zorina A, Steuer R, Červený J, Quantitative insights into the cyanobacterial cell economy, eLife, 8, 446179, 2019, doi:10.7554/eLife.42508.